PHYSICAL REVIEW A VOLUME 35, NUMBER 9 MAY 1, 1987

Measurement of KrF-laser—plasma x-ray radiation from targets with various atomic numbers

R. Popil, P. D. Gupta,* R. Fedosejevs, and A. A. Offenberger
Department of Electrical Engineering, University of Alberta, Edmonton, Canada T6G 2G7
(Received 15 October 1986)

Measurements of the x-ray conversion efficiency ($h\nu \geq 100$ eV) for a KrF-laser—produced plasma are reported. Planar targets with atomic numbers varying from 4 to 82 were irradiated by moderate intensities ($< 10^{13}$ W/cm^2) of 0.25-μm KrF-laser light and the resulting emission was observed by several detectors sensitive to x-ray photon energies from 100 eV to 15 keV. Most of the radiation appeared as xuv and was measured by x-ray diodes to obtain the conversion efficiency as well as the angular distribution of the emission. The x-ray emission both above and below 1 keV was found to display marked variation with atomic number, as successive atomic shells are ionized. These measurements are supplemented by spatial and temporal observations of the keV x-ray emission which also show variations with target atomic number.

I. INTRODUCTION

The conversion of laser energy to x rays has been one of the primary objectives of many laser-plasma interaction experiments since the inception of this field of research.[1–7] Earlier investigations were principally concerned with the conversion of laser energy to x rays in the photon-energy range of greater than 1 keV, motivated by the application of these x rays to lithography[8,9] and radiography.[10] More recently, the emphasis has shifted to soft (sub-keV) x-ray generation since a significant fraction of laser energy can be converted into radiation in this energy range.[11,12,13] In particular, for high-Z laser plasmas where the heat fluxes transported by radiation and electrons may be comparable, the soft x-ray radiation can influence ablation through radiative energy transport.[14] Soft—x-ray generation from high-Z targets has also been pursued as a means of achieving more uniform compression in laser fusion experiments,[15] as a source of indirect drive of fusion "cannonball" targets and as a pump for potential x-ray lasers.[16,17]

Moreover, the high efficiency of x-ray conversion has made plasmas produced by ultraviolet laser radiation a most efficient and convenient source of high-intensity x-ray fluxes for the applications listed above. Comparative studies have demonstrated that the conversion efficiency increases considerably with shorter laser wavelengths.[18,19,20] However, few results have been reported thus far at 0.27 μm wavelength[19,20,21] (obtained from frequency multiplication of Nd:glass laser light), and these have been restricted to x-ray conversion using gold and aluminum targets. Use of KrF-laser radiation at 0.25 μm is of interest in this regard since it has a considerably higher efficiency than Nd:glass lasers for generating short wavelength radiation. To date, reports of x-ray conversion from KrF-laser—produced plasmas[22,23] have been limited to aluminum targets and to x rays above 1 keV energy.

In this paper, we report the first detailed measurements of total x-ray conversion for varying atomic number targets using a short pulse KrF laser system. Measurements of the sub-keV and keV emission from planar targets were performed using a variety of detectors, each suited for a particular x-ray photon energy range. The energy conversion efficiency in each selected x-ray energy band was determined as a function of atomic number and incident laser energy using known quantum efficiencies. In addition, the spatial and temporal variations of the keV emission with target Z were examined to assess the role of lateral energy transport and radiation cooling. Angular distributions of the x-ray emission for Au and Al targets are reported which appear to be at variance with the Lambertian cosine law expected from an optically thick plane surface emitter.

II. EXPERIMENTAL DETAILS

A. Laser system and targets

Brillouin compressed KrF-laser pulses[24] of 1.8 ns FWHM and energies up to 2 J were focussed by a 70 cm focal length $f/10$ plano-convex lens onto targets with atomic numbers ranging from $Z = 4$ to 82. The focal spot intensity distribution was monitored by an equivalent focal plane image system coupled to a uv video digitizing system. The average equivalent radius of the 70% energy containing contour was ~ 50 μm and intensities using 70% of the incident energy within this contour ranged from 2.5—8×10^{12} W/cm^2. Intensities were varied by changing the incident laser energy which ranged from a 300 mJ up to 2 J.

The majority of the data is centered around 1 J on target and consists of approximately 600 laser shots on 19 different atomic number targets consisting of foil samples ≥ 10 μm in thickness adhered to large aluminum slabs. The target position was adjusted to provide a fresh surface at the laser focus prior to each laser shot. The purity of each target sample was 99.9% or better and all but the lithium targets were free of thick oxide layers. The effect of oxide layers in our experiments was tested by preheating the target surface by firing several defocussed laser beam shots on the same focal spot at an energy density of 10 J/cm^2, prior to laser irradiation at high intensity. No observable difference in x-ray emission was detected after such surface cleaning. The lithium targets were treated as oxygen ($Z=8$) since the relatively high keV emission suggested the unavoidable presence of an oxide layer. Similarly, the Teflon target $[(CF_2)_x]$ was assumed to have $Z=9$ since the higher atomic number fluorine would be the dominant x-ray emitting ion species in the plasma. The targets and the x-ray detectors were positioned in a vacuum target chamber maintained at 2×10^{-5} Torr (or better) by means of an oil diffusion pump in series with a dry ice cold trap to prevent backstreaming of pump oil into the chamber.

The optimum focal position of the target slab with respect to the focussing lens was determined by observing the ratio of the soft—x-ray intensity to the laser energy as a function of target position. The uncertainty in the best focus position determined in this manner was ±0.5 mm and was maintained throughout the course of the experiments by He-Ne laser alignment of the axial position of the target slab prior to each shot.

B. Geometry of the detectors

The experimental setup is shown in Fig. 1. Four x-ray diodes were used to monitor the soft—x-ray emission. A *p-i-n* diode and two scintillator-photomultiplier (SPM) detectors were used to observe hard x rays (≥ 1 keV). The *p-i-n* diode and x-ray diodes (designated as XRD 2, 3, and 4 in Fig. 1) were arranged so that each detector observed x rays in a small cone centered at 19° with respect to the target normal, thereby avoiding any relative anisotropy of emission. Emission anisotropy was monitored by XRD 1 that was positioned at an angle of 55° with respect to target normal. The *p-i-n* diode was placed inside an extension tube 3 m from the target in order to prevent saturation of this detector by the high x-ray fluences from some of the targets. X-ray diodes 1, 2, and 3 were positioned 13 cm away from the target and XRD 4 was placed 40 cm away. Not shown in Fig. 1 are the x-ray pinhole camera and x-ray streak camera used for spatial and temporal resolution of keV x rays.

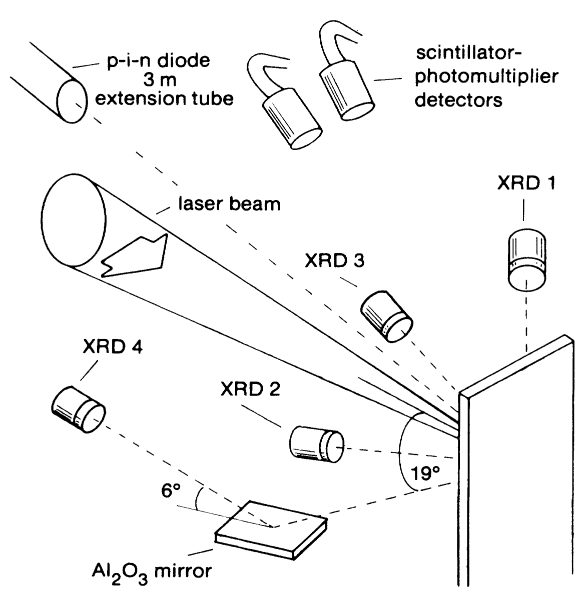

FIG. 1. Schematic diagram of the experimental setup inside the vacuum target chamber. Aperturing for the aluminum mirror is not shown for clarity.

The x-ray diodes were biplanar with dry machined Al photocathodes as specified in Ref. 24. Temporal stability of such photocathodes over several months, reported to be good to within 20%,[25,26] was verified by comparing responses of used, newly machined and Al vacuum deposited photocathodes. Differences no greater than 19% in the relative calibrations were found. The diodes were periodically cross calibrated throughout the course of the experiments using a laser-produced aluminum plasma as the x-ray source and having all the diodes mounted together in a cluster with similar Formvar filters. Flat stainless steel mesh which had 31% transmission was used as the anode material. The influence of uv light from the plasma on the measurements was found to be negligible.

The x-ray diodes were biased at 1 kV through a 90 cm charging line and the signals were observed on Tektronix 7104 oscilloscopes. The overall time resolution of the system as determined from the observation of 0.5 ns hard—x-ray bursts was better than 1 ns. The anode to cathode distance was 0.127 cm, and the photocathode diameter 1.27 cm. The calculated space charge-limited signal level[27] for this x-ray diode system is 185 V into a 50-Ω load. Typically, x-ray detector (XRD) signals were observed to be smaller than 100 V.

C. Detector response

To obtain the x-ray conversion efficiency in the most straightforward manner detectors with flat responses are desired. A *p-i-n* diode with a 10 μm Be foil filter was used to provide an essentially flat response for the 1—10 keV range. X-ray diodes consisting of Al photocathodes filtered with Formvar filters[28] of thickness ≤ 1 μm show considerable variation in the response in the soft—x-ray range 100—1000 eV. Since there are two distinct response regions on either side of the carbon K edge at 283 eV, the x-ray energy content in the lower energy band (100—280 eV) was separately measured using a Formvar filtered XRD together with a high energy cutoff x-ray mirror that did not reflect x rays >300 eV. Separate assumed flat responses were then used to obtain the x-ray conversion in the two sub-keV ranges.

An example of the two response regions is given in Fig. 2 by the solid curve which is the calculated response of XRD 3 obtained by convoluting transmission of a 1.1 μm Formvar filter with the quantum efficiency of an Al photocathode. The quantum efficiency of the prepared Al photocathode was taken from the measured values of similarly prepared photocathodes.[25] The Formvar mass attenuation coefficients were compiled from data presented by Henke *et al.*,[29,30,31] Viegele[32] and supplemented by measured values from Day *et al.*[25] in the photon energy range of 100—240 eV. The Formvar filter thicknesses

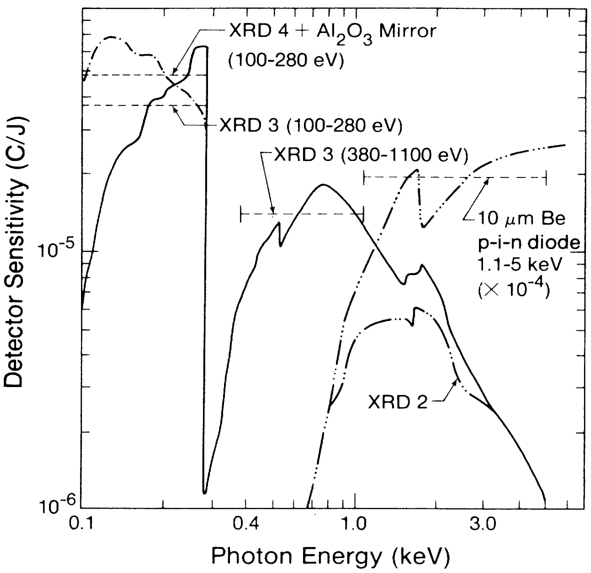

FIG. 2. Response of the x-ray detector channels (—·—·—·) XRD 4—0.5 μm Formvar filter convoluted with Al_2O_3 mirror reflectivity and aluminum photocathode; (— — —) XRD 3—1.1 μm Formvar and Al photocathode; (—··—) XRD 2—0.91 μm Formvar + 2 B-10 foils; (— · · · —) *p-i-n* diode filtered with 10 μm Be.

were determined by observation of transmission maxima obtained from visible and near ir spectrophotometric scans of the various filters. A dashed line through the solid curve of Fig. 2 shows the average response in the x-ray energy range 380—1100 eV which is 1.43×10^{-5} C/J. Average responses were calculated by integrating the response curves and dividing the result by the energy interval of interest. The lower bound on the 380—1100 eV energy range is the corresponding photon energy where the response is $1/e$ times its maximum value beyond the carbon K edge. The upper bound was taken as 1100 eV since the x-ray emission above this value was measured by the *p-i-n* diode. Thus, XRD 3 was considered to have a flat response in the range 380—1100 eV. The average response of XRD 3 in the 100—280 eV region is also shown in Fig. 2 and this value is used to account for the contribution to the XRD 3 signal from the measured radiation in this region.

To obtain a flat response in the photon energy range of 100—280 eV, XRD 4 was used in conjunction with a high energy cutoff x-ray mirror.[29,33] The mirror was arranged to give incident and reflecting glancing angles of 105 mr between XRD 4 and the plasma, and positioned so that a narrow cone of rays propagating at 19° with respect to target normal would reflect off the mirror into the detector. For the sake of clarity, an aperture used for defining the optical geometry, as well as a positioning lance used for alignment, are not shown in Fig. 1.

The high—energy-cutoff Al_2O_3 mirror was made from 99.99% pure Al, diamond turned on a microsurface lathe and subsequently anodized[34] to form an oxide coating approximately 70 nm thick. The mirror reflectivity at 105 mr glancing angle was taken from Ref. 32. The convoluted response of the 0.5 μm thick Formvar filter of XRD 4, Al_2O_3 mirror and aluminum photocathode is shown as the dot-dashed curve in Fig. 2. The dashed line is the nominal average response in the 100—280 eV photon energy range, 4.88×10^{-5} C/J, which was used for the observed charge yields from XRD 4. Thus, energy conversion in the range 100—280 eV is obtained directly from the integrated charge observed from XRD 4 using this average flat response.

The energy conversion efficiency in the photon energy range of 380 to 1100 eV was obtained by subtraction of charge yields[26,35] from diodes 2 and 4 (whose sensitivities are outside of this energy window) from the charge yield obtained from XRD 3. The detector XRD 2 has a response of 1.1—5 keV,[36] as shown in Fig. 2. Variations in the individual Formvar filter thicknesses for the various diodes were incorporated into the subtraction procedure. The resulting charge yield obtained in this manner was then converted to x-ray energy by the average value of 1.43×10^{-5} C/J as indicated in Fig. 2.

The response of the *p-i-n* diode used to derive the energy conversion in the 1.1—10 keV range was assumed to be flat to 10 keV and was 0.20 C/J. (This average response for the *p-i-n* diode is actually weighted for the 1.1—1.5 keV range since negligible radiation is expected beyond 5 keV.) The SPM detectors were oriented to observe angles greater than the 19° conical angle and to monitor the x-ray radiation beyond 3 keV. The ratio of the signal intensities from the SPM detectors were used to estimate the coronal electron temperature. Table I summarizes the characteristics of the detectors, their associated filters, sensitive pho-

TABLE I. Summary list of the detector characteristics, their respective filters, response windows, and assumed sensitivities.

Detector	Filter	Response window	Sensitivity (C/J)
XRD 1	0.5 μm Formvar	100 eV-5 keV	
XRD 2	2× B-10 + 0.9 μm Formvar	1.1 keV-5 keV	
XRD 3	1.1 μm Formvar	380—1100 keV	1.43×10^{-5} [a]
XRD 4	0.5 μm Formvar + mirror	100—280 eV	4.88×10^{-5}
p-i-n diode	10 μm Be	1.1—10 keV	0.2 C/J
SPM 1	9 μm Al	3.8—15 keV	
SPM 2	22 μm Al	5.2—15 keV	

[a]Response used after charge subtraction procedure (see text).

ton energy windows, and responses as used in determining energy conversion.

III. RESULTS

A sample of the observed voltage signal from XRD 3 as a function of laser energy is shown in Fig. 3. The scatter in data is typical of that observed for all targets and can be attributed to shot-to-shot variations in laser pulselength and/or laser beam spatial quality. Typically, for a nominal fixed energy E of 0.9 J on target, mean fluctuations of 12% and 30% were observed for the pulselength and focal diameter, respectively.

Signal intensity from the x-ray diodes monitoring emission below 1 keV varies as $E^{1.0-1.4}$ for the various targets used. In contrast, the scaling observed for emission above 1 keV was considerably greater with incident laser energy, varying as $E^{1.4-3.4}$. This faster scaling can be explained by the dependence of x-ray emission intensity I_x, on electron temperature ($I_x \propto \exp(-h\nu/kT_e)$. Emission of significant x-ray radiation in the keV range only occurs for electron temperatures of several hundred eV in the plasma and is therefore more critically dependent on the incident laser intensity to produce these required temperatures.

The pulsewidth of the soft—x-ray signals varied from $\sim$3—4 ns FWHM for low-Z elements to $\sim$2 ns FWHM for high-Z elements. In contrast, x-ray signals for energy >1 keV, as observed by XRD 2, had much shorter pulsewidths ranging from $\sim$1—2 ns. x-ray streak camera observations[38] (20 ps resolution) of hard x-rays transmitted through a 10 μm Be filter showed that the ratio of the FWHM duration of the x-ray emission to the laser pulse width varied from 0.8 for low-Z elements to 0.3 for high-Z elements at approximately the same laser intensity. The relatively shorter duration of both soft— and hard—x-ray emission for high-Z targets is thought to be due to increased cooling of the plasma caused by higher radiation losses since cooling due to hydrodynamic expansion would be comparatively less important for high-Z targets.

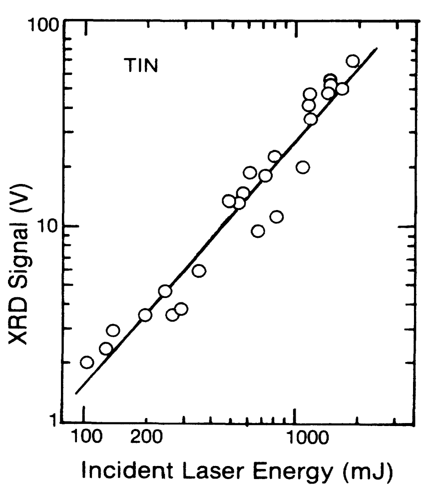

FIG. 3. Voltage signals from XRD 3 as a function of laser energy for a tin target. The line is a least-squares fit indicating a dependence on laser energy of $E^{1.3}$.

Data from the p-i-n diode and SPM detectors showed a large modulation of keV x-ray intensity as a function of atomic number Z. The dependence of keV x-ray emission on target Z observed using SPM detectors filtered by Al foils of thickness 9 and 22 μm for a nominal energy of 0.93 J on target is shown in Figs. 4(a) and 4(b), respectively. (The corresponding cutoff energies defined from $1/e$ transmission through the two filters are 3.8 and 5.2 keV.) Three distinct peaks in Figs. 4(a) and 4(b) are observed, due to enhanced radiation from bound-bound and free-bound transitions to the available atomic shells. The intensity of these transitions vary with atomic number for a given electron temperature and density. These peaks in x-ray conversion occur when the internal energy of the plasma can produce a large number of excitations to a given shell, determined by the atomic structure of a particular target element. The three peaks observed in Figs. 4(a) and 4(b) are thus expected to be due to transitions to K, L, and M shells, respectively. The location in Z of the observed peaks is consistent with previous work using longer wavelength lasers[2,6,7,39] and supports the observations made in Ref. 6 that locations of the keV emission peaks change only slightly for widely varying laser irradiation conditions.

The SPM measurements provided an estimate of the electron temperature based on the foil ratio technique. Coronal ionization equilibrium calculations for all targets were performed for the free-free and free-bound radiation transmitted through the foil absorbers as a function of the electron temperature. Since the cutoff energies of the absorbers used were 3.8 and 5.2 keV, it is expected that a reasonable estimate of the coronal electron temperature can be obtained for those target elements where line radiation above 1 keV is not dominant. Analysis of the data showed that C, Li(O), CF_2(F), Al, Ti, Fe, Mo, Cd, Yb, and Au targets produced electron temperatures in the range of 200—300 eV. These electron temperatures did not show any obvious dependence on Z, an observation that is consistent with that of Glibert *et al.*[6] Simple self-regulating model[40] considerations suggest that for a given laser intensity, the electron temperature should increase with Z and atomic mass. The observation that the electron temperature does not increase for higher-Z targets is consequently attributed to increased energy losses due to increased ionization and radiation in high-Z plasma.[41]

The x-ray energy conversion efficiency in the 1.1—10 keV range as deduced from p-i-n diode measurements is shown in Fig. 4(c). Three peaks in x-ray emission as a function of atomic number are once again evident. For 0.93 J on target (5×10^{12} W/cm^2) a maximum conversion of 1.3$\pm$0.4% is observed (for Ni targets). Estimation of the conversion efficiency in this photon energy range has assumed isotropic emission into 2π sterradians since it is expected that hard x-ray emission should largely emanate from the extended hot coronal region of the plasma and be optically thin. However, it has been demonstrated in another experiment[42] that the intense resonance line emission of Al XII ions (1.6 keV) follows a cosine angular distribution whereas less intense line radiation from the Al plasma is considerably more isotropic. Hence, the keV x-ray conversion in Fig. 4(c) should be taken as an upper

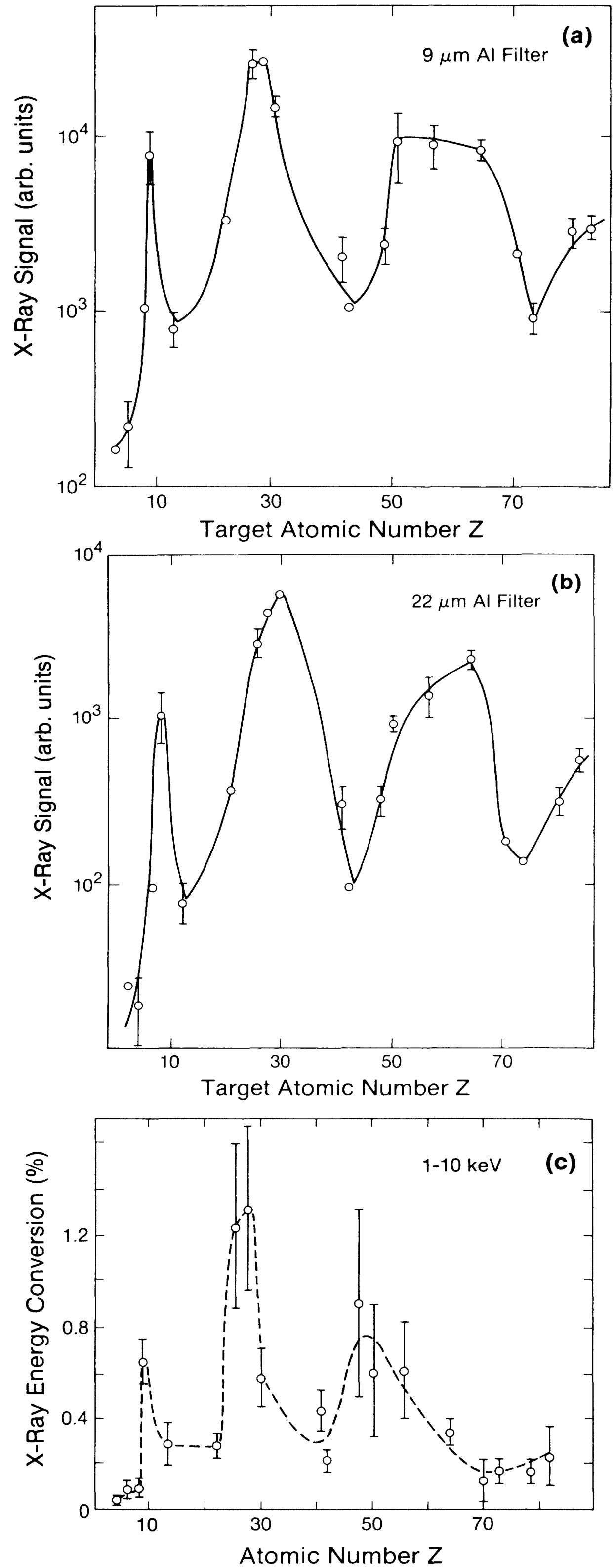

FIG. 4. KeV x-ray signal versus target atomic number at 0.93 J on target: (a) SPM detector with 9 μm Al filter; (b) SPM detector with 22 μm filter; (c) x-ray energy conversion measured by the *p-i-n* diode channel. The curves are intended as visual guides only.

bound; it is nonetheless a small contribution to the overall energy conversion.

Results of x-ray conversion measurements for the two soft–x-ray energy bands, 100–280 eV and 380–1100 eV, as a function of target atomic number for a laser intensity of 5×10^{12} W/cm^2 are shown in Fig. 5(a). A comparison of these results with those of the keV x-ray emission [Fig. 4(c)] clearly shows the dominance of the soft–x-ray energy radiation. A pronounced increase in emission with atomic number is evident for the 380–1100 eV band. For comparison with previous work,[19,20,21,26] a cosine distribution was assumed in calculating conversion efficiencies in the sub-keV range. The error bars shown in Fig. 5(a) and 5(b) are principally due to scatter in the XRD data and the smooth curves in Fig. 5(a) and 5(b) are visual guides only. The total x-ray energy conversion efficiency, given by the sum of conversions in the various bands, yields the results shown in Fig. 5(b). The data are plotted for an average 0.93 J on target and, in addition, best fit curves are plotted for 0.47 and 1.4 J data. It is observed that

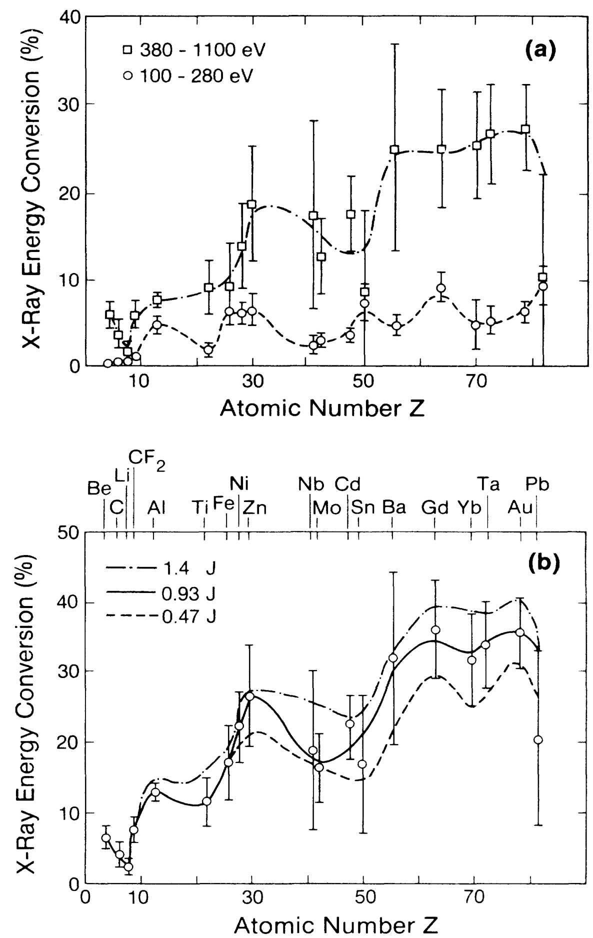

FIG. 5. (a) X-ray energy conversion in the sub-keV bands 100–280 eV (lower curve) and 380–1100 eV (upper curve) for 0.93 J average energy on target. (b) Total x-ray energy conversion efficiency as a function of target atomic number. The data points and solid curve are for 0.93 J on target, best fit curves are shown for 0.47 and 1.4 J data as indicated.

over our limited intensity range of $2.5-8\times10^{12}$ W/cm^2, the total x-ray energy conversion increases slightly with laser intensity for high atomic numbers. The peak conversion efficiency at 8×10^{12} W/cm^2 is 40.6 ± 7.5 % for Au targets and 14.5 ± 2.5 % for Al targets.

The angular distribution of the sub-keV x-ray emission relative to the other detectors was monitored during the conversion measurements by XRD 1 placed at an angle of 55° with respect to target normal. Data collected for Zn, Fe, Ni, and Au targets suggested that the soft—x-ray emission was considerably more isotropic than a cosine distribution. If the emission were completely isotropic, the x-ray yield would be 1.89 times greater than the values plotted in Fig. 5(b). Emission isotropy was examined in detail using the x-ray diodes placed at angles of 12°, 19°, 40°, 55°, 63°, and 78° to the target normal. Four x-ray diodes were used in two different geometries to cover all the angles. The x-ray signals are plotted logarithmically versus the cosine of the angle in Figs. 6(a) and 6(b) to determine the azimuthal dependence. For the case of Al plasma, Fig. 6(a), a least-squares fitting gives $(\cos\theta)^{0.76}$ and for Au plasma, Fig. 6(b), the fit is $(\cos\theta)^{0.33}$. An angular dependence of $(\cos\theta)^{0.5}$ has recently been observed by Kodama *et al.*[20] for 0.27 μm laser irradiated Au targets. Incorporating the observed $\cos\theta$ scalings for total conversion efficiency into 2π sr, we find that the Al emission increases by 1.08 times and that for Au by 1.46 times. The maximum observed conversion efficiencies for Al and Au at 8×10^{12} W/cm^2 are then $15.7\pm2.75\%$ and 59.3 ± 11 %, respectively.

A pinhole camera with a 10 μm thick Be filter was used to observe the keV x-ray emission from Al, Au, Gd, and Fe targets. The camera was oriented at 45° to target normal and x-ray images with a magnification of $3\times$ and spatial resolution of 12.5 μm were recorded on Kodak DEF film. Irregular features observed in some laser focal spots were well reproduced by similar features in the pinhole x-ray images. Good correspondence between the 0.2 ND above fog density contour diameter and the 70% energy containing contour were obtained for the Fe and Gd targets. The average lateral x-ray image dimension for the iron target was 15% larger than the average 70% energy containing focal diameter while for Gd it was 14% smaller. In contrast, the x-ray image diameters for Al and Au targets were 50% smaller than the focal diameter. That the Fe target produced the largest x-ray images is taken to reflect the fact that iron is the most efficient keV x-ray emitter out of the four selected targets together with the observation that the electron temperature does not vary significantly with Z for moderate laser intensities.

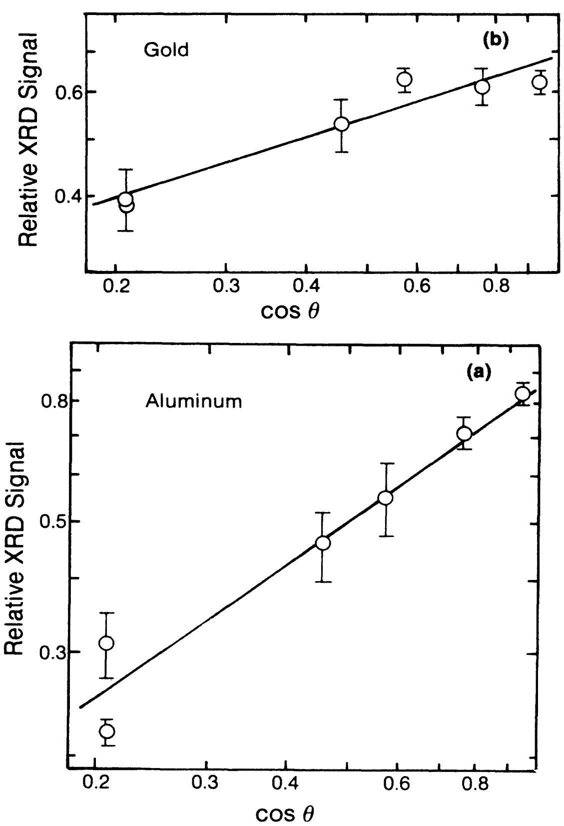

FIG. 6. Angular distribution of sub-keV x-ray emission from (a) aluminum and (b) gold plasmas. The relative signal of the XRD detectors is plotted logarithmically versus the cosine of the angle from target normal. Straight lines are least-squares fittings.

IV. DISCUSSION

In this section, the effect of nonuniform responses of the filtered x-ray diodes in estimating x-ray conversion efficiency will be assessed. A discussion of the significance of the x-ray conversion results and their scaling with laser intensity, the angular emission dependence of soft—x-ray emission and the effect of lateral energy transport on measurements will follow.

To determine the conversion efficiency accurately, the emission spectrum must be measured and the detector responses can then be adjusted accordingly. It is expected that a large part of the x-ray emission will be in the form of line emission in one or more bands.[13,39] These bands shift in wavelength with varying atomic number and, thus, detailed variations from one element to the next in our calculated x-ray yield may be due in part to the nonuniform spectral response of our detectors. However, as a number of elements are measured and the peak emission bands sweep across the detector channels, the average trend in x-ray conversion efficiency found by averaging over a number of neighboring elements should be fairly accurate.

An indication of the effect of nonuniform spectral response of the detectors on x-ray conversion calculations can be obtained by convoluting a blackbody emission spectrum with the assumed flat and actual responses for the two sub-keV bands. Although the bulk of the emitted radiation may arise from limited regions of the plasma, it is not possible, in general, to model the spectrum of emitted radiation by a single temperature Planckian distribution because of widely varying conditions of temperature and density in the plasma.[26]

A previous study[41] of Au plasma ablation by KrF laser pulses indicated the formation of a two component plasma which was inferred to correspond to a high-temperature, low-density absorption region and a low-temperature, high-density radiation heated region. The temperatures of these two components are estimated to be 200 and 75 eV, respectively. The low-temperature, high-density region would be optically thick, and in addition, the 200 eV coronal region of the plasma may also be optically thick, particularly for the sub-keV radiation emitted in the N and O bands. That the coronal region contributes significantly to the total measured radiation can be noted from the observation that if the emission spectrum were truly characterized by blackbody emission at a single temperature of 75 eV, then the amount of radiation observed in the 100—280 eV band should considerably exceed that seen in the 380—1000 eV range. As seen in Fig. 5(a), however, radiation in the 380—1100 eV range clearly dominates.

Assuming a 75 and 200 eV blackbody spectrum we calculate, utilizing the assumed flat responses, that in the 100—280 eV range the conversion efficiency is underestimated by factors of $1.02\times$ and $1.09\times$, respectively. For the 380—1100 eV range, calculations show that the conversion efficiency is underestimated by $1.3\times$ in the case of a 75 eV blackbody but only by $1.02\times$ in the case of a 200 eV blackbody. Thus, if the soft—x-ray spectrum is comprised predominantly of a low-temperature blackbody distribution, then the calculated conversion efficiencies, assuming flat responses, are underestimated in the 380—1100 eV band. Overall, the calculated conversion values give a lower bound on the total x-ray conversion efficiency due to the relatively small detector response in the photon energy range 280—380 eV.

X-ray conversion estimates obtained from these measurements with x-ray diodes are in good agreement with results obtained from an x-ray foil calorimeter. The foil calorimeter responds up to 850 eV, beyond which there is significant transmission of x rays through the thin foil element. Assuming a $\cos\theta$ distribution, the x-ray calorimeter conversion efficiencies at laser irradiance of 5×10^{12} W/cm^2 for aluminum and gold are $14\pm4\%$ and $31\pm8\%$, respectively, in experimental agreement with comparable values obtained from the XRD data [Fig. 5(b)]. It is noted, however, that both sets of measurements do not cover the entire x-ray spectrum and thus are underestimations of the total conversion.

The x-ray conversion values measured in the present experiment appear to increase with laser intensity in the range of $2.5-8\times10^{12}$ W/cm^2. This is consistent with observations of Nishimura *et al.*[18] at 0.35 μm irradiation, in which the x-ray energy conversion for gold disk targets was seen to increase from 20% to 40% in the intensity range $1-10\times10^{12}$ W/cm^2. A one-dimensional plane model that includes detailed atomic physics and radiation transport (Duston *et al.*[43]) for 0.35 μm radiation, also indicates an increase of conversion efficiency with laser intensity up to 10^{14} W/cm^2 and a subsequent decrease around 10^{15} W/cm^2 Since modelling[19] for low intensities ($<10^{14}$ W/cm^2) suggests that the underdense coronal plasma plays a dominant role in overall x-ray emission, the increase of x-ray conversion with laser intensity may be attributed to the simultaneous increase of the dimensions and temperature of the coronal plasma.

We now compare the conversion efficiencies measured in our experiment with those reported for 0.27 μm laser irradiation obtained using frequency multiplication of Nd:glass lasers, although a direct comparison is difficult in view of the differences in laser pulse duration, focal spot size, and laser intensity. For the case of Al and Au KrF-laser—produced plasmas, conversion efficiencies taking into account the measured $\cos\theta$ distributions, are determined to be $15.7\pm2.7\%$ and $59.3\pm11\%$, respectively, for 8×10^{12} W/cm^2. While the conversion efficiency for Au plasmas in our experiment is somewhat lower than values obtained in other experiments,[19,20] reasonable agreement is found for Al plasma.[20,21] For instance, a conversion efficiency of 85% at 9×10^{13} W/cm^2 has been measured in gold disk irradiation at 0.26 μm (1 ns pulse, 1500 μm focal spot),[19] and Kodama *et al.*[20] have observed a conversion of 80% at 2.4×10^{13} W/cm^2 (400 ps pulse, 150 μm spot size).

The smaller conversions observed in our experiment may be qualitatively accounted for by the following considerations. (1) For the small focal spot of 100 μm and long pulse duration of ~2 ns, hydrodynamic expansion of the plasma would be significant during the laser pulse. Consequently, a larger fraction of the laser energy would go into the kinetic energy of ions, leaving a smaller energy available for x-ray emission. (2) The conversion ratios measured in our experiments were obtained at smaller laser intensities than other experiments, and for our laser intensity range the conversion increases with laser intensity. (3) Lastly, the present estimates only give a lower bound since the contribution of the spectral region 280—380 eV is not included due to the negligible response of the x-ray diodes in this range, as discussed earlier.

The angular distribution of soft—x-ray emission for both Al and Au targets is more isotropic than a $\cos\theta$ behavior expected for emission from a planar disklike surface of an optically thick plasma. Observations in other experiments[20,44] on gold plasma have also indicated angular distributions to be more isotropic than $\cos\theta$. In planar target experiments, this behavior can be expected if a significant fraction of the measured radiation is contributed either by an optically thin emission region or by the outer regions of the plasma. Both of these effects would enhance the contribution of the coronal region to the overall x-ray emission, an inference made earlier from the measured relative energy content in the two sub-keV spectral bands. Furthermore, for our experimental conditions, including small focal spot size, spherical expansion of the outer corona can be expected, thus favoring isotropic emission. The increase in radiation isotropy for gold as compared to aluminum would suggest that the emitting region for gold lies more in the coronal region than in the overdense region, as indicated by a 2D simulation[19] for 0.27 μm light at low intensity. Hence, the Al plasma soft—x-ray radiating region should be more disklike than that for the Au plasma and therefore shows a predominantly $\cos\theta$ emission distribution.

X-ray imaging of keV emission has been used previously to assess the role of lateral energy transport in 0.53 μm irradiation experiments[26,44] which showed that the spatial extent did not significantly exceed the focal spot dimension. Similar observations have been made in the present experiment, showing keV x-ray images not significantly exceeding the focal spot size. On the other hand, analyses of ion diagnostic data from KrF laser irradiated Al targets[45] have suggested that there is significant lateral energy spread. Moreover, time-resolved picosecond dye laser shadowgraphy[46] of the tangential expansion of the plasma has shown that at the time of the peak of the laser pulse, the lateral 0.01 n_{cr} density contour (n_{cr} is critical density) can be twice as large as the focal diameter, thus indicating a peripheral tenuous cold plasma region resulting from lateral transport. Lateral energy transport, by cooling the plasma, would lower the overall total x-ray conversion efficiency. Therefore, the lower conversion efficiencies observed in our experiments may also be due to 2D effects.

V. CONCLUSIONS

The total x-ray energy conversion for KrF-laser—irradiated targets has been measured in sub-keV and keV photon energy ranges for 19 elements. X-ray conversion in the intensity range of $2.5-8\times10^{12}$ W/cm^2 was observed to increase the laser intensity. X-ray energy conversion for Au and Al were determined to be $40.6\pm7.5\%$ and $14.5\pm2.5\%$, respectively, at 8×10^{12} W/cm^2 assuming a cosine angular distribution of x-ray emission. A study of the radiation isotropy showed that the Au plasma x-ray emission is relatively more isotropic implying a 2π Au conversion of $59.3\pm11\%$ and for Al $15.7\pm2.7\%$. The relative emission isotropy and the measured distribution of radiation in the sub-keV range implies that the dominant x-ray emitting zone for the Au plasma lies in the coronal region.

The conversion above 1 keV was found to be small, $<2\%$, in comparison with that measured in the sub-keV bands. Pronounced modulations in the keV x-ray emission intensity with target Z were observed which can be related to the atomic shell structure. Lower than expected electron temperatures and relatively smaller durations of x-ray emission from high-Z plasmas are consistent with higher radiation losses in these plasmas. X-ray pinhole camera images of the keV emitting corona showed lateral dimensions comparable to the focal diameter but other evidence suggests that lateral energy transport may be a significant energy loss in our experiment, consequently limiting the x-ray energy conversion.

ACKNOWLEDGMENTS

The authors would like to acknowledge the technical assistance of B. Harwood, K. Houston, and A. Haromy throughout the duration of the experiments. In addition, the assistance of D. Vick, who was involved in the measurement of filter thicknesses, is gratefully acknowledged. This work is supported by the Natural Sciences and Engineering Research Council of Canada.

---

*On leave from the Bhabha Atomic Research Center, Trombay, Bombay 400085, Maharashtra, India.

[1]K. Eidmann, M. H. Key, and R. Sigel, J. Appl. Phys. **47**, 2402 (1976).
[2]H. Pepin, B. Grek, F. Rheault, and D. J. Nagel, J. Appl. Phys. **48**, 3312 (1977).
[3]D. J. Nagel, P. G. Burkhalter, C. M. Dozier, J. F. Holzrichter, B. M. Klein, J. M. McMahon, J. A. Stamper, and R. R. Whitlock, Phys. Rev. Lett. **33**, 743 (1974).
[4]P. Burkhalter, U. Feldman, and R. Cowan, J. Opt. Soc. Am. **64**, 1058 (1974).
[5]L. Chase, W. Jordan, J. Perez, and R. Johnston, Phys. Rev. A **13**, 1497 (1976).
[6]K. M. Glibert, J. P. Anthes, M. A. Gusinow, and M. A. Palmer, J. Appl. Phys. **51**, 1449 (1980).
[7]R. D. Bleach and D. J. Nagel, J. Appl. Phys. **49**, 3832 (1978).
[8]D. J. Nagel, M. C. Peckerar, R. R. Whitlock, J. R. Grieg, and R. E. Pechacek, Electron. Lett. **14**, 781 (1978).
[9]D. J. Nagel, C. M. Brown, M. C. Pecherar, M. L. Ginter, J. A. Robinson, T. J. McIlrath, and P. K. Caroll, Appl. Opt. **23**, 1428 (1984).
[10]M. H. Key, C. L. S. Lewis, J. G. Lunney, A. Moore, T. A. Hall, and R. G. Evans, Phys. Rev. Lett. **41**, 1467 (1978); D. L. Matthews, E. M. Campbell, N. M. Ceglio, G. Hermes, R. Kaufmann, L. Koppel, R. Lee, K. Manes, V. Rupert, V. W. Slivinsky, R. Turner, and F. Ze, J. Appl. Phys. **54**, 4260 (1983).
[11]J. Mizui, N. Yamaguchi, T. Yamanaka, and C. Yamanaka, Phys. Rev. Lett. **39**, 619 (1977).
[12]J. Mizui, N. Yamaguchi, S. Takagi, and K. Nishihara, Phys. Rev. Lett. **47**, 1000 (1981).
[13]K. Eidmann and T. Kishimoto, Appl. Phys. Lett. **49**, 377 (1986).
[14]P. D. Gupta, Y. Y. Tsui, R. Popil, R. Fedosejevs, and A. A. Offenberger, Opt. Commun. (to be published).
[15]J. L. Bocher, M. Decroisette, P. A. Holstein, M. Louis-Jacquet, B. Meyer, A. Saleres, and G. Thiell, Phys. Rev. Lett. **52**, 823 (1984).
[16]R. H. Dixon and R. C. Elton, Phys. Rev. Lett. **38**, 1072 (1977).
[17]R. G. Caro, J. C. Wang, J. F. Young, and S. E. Harris, Phys. Rev. A **30**, 1407 (1984).
[18]H. Nishimura, F. Matsuoka, M. Yagi, K. Yamada, S. Nakai, G. H. McCall, and C. Yamanaka, Phys. Fluids **26**, 1688 (1983).
[19]W. C. Mead, S. V. Coggelshell, S. R. Goldman, E. K. Stover, P. D. Goldstone, A. Hauer, J. M. Kindel, and L. Montierth, Los Alamos National Laboratory Report No. LA-UR-86-300, 1985 (unpublished).
[20]R. Kodama, K. Okada, N. Ikeda, M. Mineo, K. A. Tanaka, T. Mochizuki, and C. Yamanaka, J. Appl. Phys. **59**, 3050 (1986).
[21]H. Pepin, R. Fabbro, B. Faral, F. Amiranoff, J. Virmont, F. Cottet, and V. P. Romain, Phys. Fluids **28**, 3393 (1985).
[22]P. D. Gupta, R. Popil, R. Fedosejevs, and A. A. Offenberger, Appl. Phys. Lett. **48**, 103 (1986).
[23]Y. Matsumoto, M. J. Shaw, F. O'Neil, J. P. Partanen, M. H.

Key, R. Eason, I. N. Ross, E. M. Hodgson, and Y. Sakagami, Appl. Phys. Lett. **46**, 28 (1985).

[24]R. Fedosejevs and A. A. Offenberger, IEEE J. Quant. Electron. **QE-21**, 1558 (1985).

[25]R. H. Day, P. Lee, E. B. Saloman, and D. J. Nagel, J. Appl. Phys. **52**, 6965 (1981).

[26]T. Mochizuki, T. Yabe, K. Okada, M. Hamada, N. Ikeda, S. Kiyokawa, and C. Yamanaka, Phys. Rev. A **33**, 525 (1986).

[27]R. B. Spielman and J. P. Anthes, in *Low Energy X-Ray Diagnostics (Monterey, 1981),* Proceedings of the Topical Conference on Low Energy X-ray Diagnostics, AIP Conf. Proc. No. 75, edited by D. T. Attwood and B. L. Henke (AIP, New York, 1981), p. 278.

[28]R. Popil, A. Harmoy, R. Fedosejevs, and A. A. Offenberger, Rev. Sci. Instrum. **57**, 2625 (1986).

[29]B. L. Henke, P. Lee, T. J. Tanaka, R. L. Shimabukuro, and B. K. Fujikawa, At. Data Nucl. Data Tables **27**, 1 (1982).

[30]B. L. Henke and E. S. Ebisu, Adv. X-ray Anal. **17**, 150 (1973).

[31]B. L. Henke and R. L. Elgin, Adv. X-ray Anal. **13**, 639 (1970).

[32]W. J. Viegele, *Handbook of Spectroscopy Vol. I,* edited by J. W. Robinson (CRC, Florida, 1974), p. 28.

[33]V. Rehn, in *Low Energy X-Ray Diagnostics (Monterey, 1981),* Proceedings of the Topical Conference On Low Energy X-ray Diagnostics, AIP Conf. Proc. No. 75, edited by D. T. Attwood and B. L. Henke (AIP, New York, 1981), p. 162.

[34]L. Holland, *Vacuum Deposition of Thin Films* (Chapman and Hall, London, 1963), p. 345.

[35]C. L. Wang, Rev. Sci. Instrum. **53**, 582 (1982).

[36]XRD 2 contains aluminized polycarbonate foil consisting of two layers of B-10 available from Alexander Vacuum Research, Inc., 278 Main St., Greenfield, Ma 01301.

[37]Quantrad Corporation, Los Angeles CA 90064.

[38]R. Popil, R. Fedosejevs, and A. A. Offenberger, Rev. Sci. Instrum. **57**, 1049 (1986).

[39]H. C. Gerritsen, H. van Burg, F. Bijkerk, and M. J. van der Wiel, J. Appl. Phys. **59**, 2337 (1986).

[40]P. Mora, Phys. Fluids **25**, 1051 (1981).

[41]P. D. Gupta, Y. Y. Tsui, R. Popil, R. Fedosejevs, and A. A. Offenberger, Phys. Rev. A **34**, 4103 (1986).

[42]L. F. Chase, W. C. Jordan, J. D. Perez, and J. G. Pronko, Appl. Phys. Lett. **30**, 137 (1977).

[43]D. Duston, R. W. Clark, and J. Davis, Phys. Rev. A **31**, 3220 (1985).

[44]W. C. Mead, E. M. Campbell, W. L. Kruer, R. E. Turner, C. W. Hatcher, D. S. Bailey, P. H. Y. Lee, J. Foster, K. G. Tirsell, B. Pruett, N. C. Holmes, J. T. Trainor, G. L. Stradling, B. F. Lasinski, C. E. Max, and F. Ze, Phys. Fluids **27**, 1301 (1984).

[45]P. D. Gupta, Y. Y. Tsui, R. Popil, R. Fedosejevs, and A. A. Offenberger, Phys. Rev. A **33**, 3531 (1986).

[46]A. A. Offenberger, R. Fedosejevs, P. D. Gupta, R. Popil, and Y. Y. Tsui, Laser Part. Beams **4**, 329 (1986).